

# Observational Aspects of Particle Acceleration in Large Solar Flares

John C. Raymond · Säm Krucker · Robert P. Lin · Vahé Petrosian

Received: 29 February 2012 / Accepted: 16 May 2012 / Published online: 12 June 2012  
© US Government 2012

**Abstract** Solar flares efficiently accelerate electrons to several tens of MeV and ions to 10 GeV. The acceleration is usually thought to be associated with magnetic reconnection occurring high in the corona, though a shock produced by the Coronal Mass Ejection (CME) associated with a flare can also accelerate particles. Diagnostic information comes from emission at the acceleration site, direct observations of Solar Energetic Particles (SEPs), and emission at radio wavelengths by escaping particles, but mostly from emission from the chromosphere produced when the energetic particles bombard the footpoints magnetically connected to the acceleration region. This paper provides a review of observations that bear upon the acceleration mechanism.

**Keywords** Solar physics: flares · Solar physics: magnetic reconnection

## 1 Introduction

Enormous numbers of particles are accelerated to high energies during solar flares. These particles contain most of the energy of large flares (Lin and Hudson 1976; Emslie et al.

---

J.C. Raymond (✉)  
Center for Astrophysics, 60 Garden St., Cambridge, MA 02138, USA  
e-mail: [jraymond@cfa.harvard.edu](mailto:jraymond@cfa.harvard.edu)

S. Krucker · R.P. Lin  
Space Sciences Laboratory, University of California, Berkeley, CA 94720, USA

S. Krucker  
Institute for 4D Technologies, School of Engineering, University of Applied Sciences  
North Western Switzerland, 5210 Windisch, Switzerland

R.P. Lin  
School of Space Research, Kyung Hee University, Suwon, Korea

V. Petrosian  
Department of Applied Physics, Stanford University, Stanford, CA 94305, USA

2005), though the energy is quickly transformed into thermal energy, bulk kinetic energy and radiation. While the source of the energy is the free energy of the magnetic field, the mechanism that transfers this energy to particles in the 10 keV to 10 GeV range is not fully understood. The dissipation of magnetic energy must be faster than the impulsive phase of a flare, which lasts roughly 10 seconds to 10 minutes, and this has posed the central problem for models of magnetic reconnection for decades. Similarly, the acceleration of particles to high energy on still shorter timescales is a major constraint for models of acceleration.

It is vital to understand both the flare and CME shock acceleration processes in order to understand the basic physics of solar eruptions and to enable predictions of energetic particle fluxes that can endanger spacecraft and astronauts. It is also important to use the solar events that can be observed in detail to understand particle acceleration in distant astrophysical objects, where far less diagnostic information is available.

A 'standard picture' of solar eruptions has evolved over the years to explain the flare/CME phenomenon and the role of energetic particles, sometimes called the CSHKP model (Carmichael 1964; Sturrock 1966; Hirayama 1974; Kopp and Pneuman 1976), even though the CSHKP model was originally designed to explain the decay phase of flares. Many of the specific aspects of this model have been questioned, but it is currently used to describe the impulsive phase as well.

An extensive review of solar flare observations, especially those at high energies, is provided by Emslie et al. (2011). In this review, we will briefly summarize the standard picture of solar eruptions. Then we describe the observations from radio to gamma-ray wavelengths, including observations that constrain the number, spectrum and composition of the energetic particles, observations that constrain the location and timing of the acceleration, and observations that constrain the parameters of the current sheets where acceleration is likely to occur. Finally, we discuss some potential problems with the standard model and some alternatives that have been proposed.

## 2 Standard Picture

To provide a context for various observations described in subsequent sections, we give here a summary of the most popular picture for large solar flares. Some problems with that picture are discussed in Sect. 5.

A large solar flare can produce in excess of  $10^{32}$  ergs of radiation from radio waves to gamma-rays. It is typically accompanied by a coronal mass ejection (CME) of comparable kinetic energy (Yashiro et al. 2005; Emslie et al. 2005; Vourlidas et al. 2010), and the flare and CME are complementary aspects of the eruptive phenomenon. However, both flares and CMEs are sometimes seen to occur alone (Yashiro et al. 2005). The energy comes from conversion of magnetic free energy stored in the corona. A simple potential field is a minimum energy state, but emergence of new magnetic flux can induce stresses, and motions at the photosphere and below can distort the field and increase its energy. Flares generally occur in regions of complex magnetic field near polarity inversion lines. A filament or flux rope seen as a coronal cavity (Gibson et al. 2010) may also be present. Both large scale shear motions and small scale turbulence at the photosphere can play significant roles (van Ballegoijen and Martens 1989).

The magnetic field strength in the flaring region is not easy to determine, and it varies rapidly with height in an active region. Brosius and White (2006) determined a field strength close to 1000 G from radio observations 12 Mm above a sunspot, while Lin et al. (2000) measured fields of 10 and 33 G at heights of 0.12 and 0.15  $R_{\odot}$  in two active regions using an

[Fe XIII] line. Extrapolations from the photospheric field using MHD or non-linear force-free field techniques typically predict strengths of order 50 Gauss at heights of 20 Mm (Savcheva et al. 2012; Sun et al. 2012). During the X4.8 flare SOL2002-07-23T00:35, the radio spectrum indicates a field strength below 200 G while a field of 500 G is required to confine the superhot component (Caspi and Lin 2010), suggesting that the bulk of the energetic electrons are higher in the corona than the superhot component (White et al. 2011).

At some point the magnetic structure becomes unstable. The trigger could be an ideal MHD instability, such as a kink instability if the field becomes too tightly wound (Török and Kliem 2005) or a torus instability (Kliem and Török 2006). Another possibility is that a region of stressed magnetic field is held down by an overlying magnetic arcade until slow, gradual reconnection reduces the strength of the overlying field and allows a rapid expansion (Antiochos et al. 1999; Lynch et al. 2008). Other classes of models suggest that photospheric motions push a pre-existing coronal flux rope from a stable to an unstable position (Lin and Forbes 2000) or that field lines that tie a magnetic loop to the photosphere are cut by reconnection. Stepping back from the specific magnetic topology, Cassak et al. (2006) and Uzdensky (2007) suggest that reconnection occurs very slowly until the structure passes from the collisional to the collisionless reconnection regime, when reconnection becomes very fast. In rare instances, a flare seems to be triggered externally, perhaps because fast mode waves from a distant flare impinge on a structure on the verge of instability (Schrijver and Title 2011).

The reconnection must be very rapid. Signatures of high energy particles such as hard X-ray emission occur during an impulsive phase that rises in seconds to a minute and lasts only a few minutes, and spikes in hard X-ray and radio emission have timescales as short as 0.1 s. If the particles are accelerated in the corona, they must be trapped long enough to be accelerated, then precipitate into the chromosphere in a very short time.

As reconnection proceeds, the CME accelerates away from the Sun. Reconnection creates or enhances a twisted flux rope (Antiochos et al. 1999; Lin et al. 2004) at the same time that it heats and accelerates the CME and produces the flare. Fast CMEs produce coronal shock waves that convert up to about 10 % of the CME kinetic energy into solar energetic particles (SEPs) (Mewaldt et al. 2008). The mechanism for that conversion is generally thought to be diffusive shock acceleration (DSA), though there are many unanswered questions, such as the origin and importance of suprathermal seed particles for the acceleration process. Particle acceleration in CME-driven shocks is discussed in Lee et al. (2012). Reconnection at the X-line produces outflows upwards and downwards, energizing the flare loops and helping to drive the CME.

The transition to a lower magnetic energy state can heat and accelerate coronal plasma and accelerate particles, but the mechanisms are not clear. Transformation of magnetic energy to particle kinetic energy by way of turbulence or electric fields in the reconnecting plasma is most commonly assumed (see, e.g., Petrosian and Liu 2004), but shrinkage of magnetic loops (dipolarization) is important in the Earth's magnetosphere and has recently been applied to solar flares, which can heat and compress the thermal plasma by means of shock waves (Longcope and Guidoni 2011). In another theory, Alfvén waves launched in the corona accelerate particles in the chromosphere (Fletcher and Hudson 2008). This theory avoids problems with the large numbers of energetic electrons accelerated in the low density corona, but it has yet to be developed in detail (see Sect. 5).

In nearly all models the magnetic free energy is released in the corona, where the plasma beta is low (i.e., the magnetic energy density is larger than the thermal energy density), leading to acceleration of particles. It is generally believed that particles on open field lines escape the reconnection region producing long wavelength radio emission, and they may be

re-accelerated at the associated CME shock and observed as SEPs, while those on closed field lines carry the energy to magnetic footpoints in the chromosphere. A tiny fraction, about 1 part in  $10^5$ , of the energy deposited in the footpoints emerges as hard X-rays, while most of the energy is lost via Coulomb collisions which heats the plasma and causes evaporation. This energy eventually emerges UV and optical continua and soft X-ray and EUV emission lines, continuing after the original energy release ceases (Fletcher et al. 2007, 2011; Dennis et al. 2011).

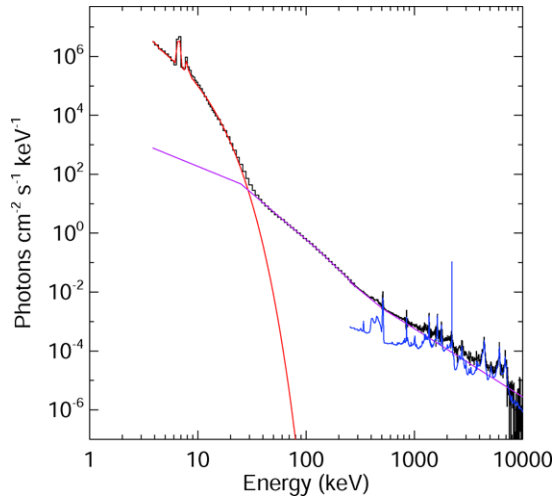
### 3 Observations and Diagnostics

Solar eruptions can be observed from radio to gamma-ray wavelengths, and electrons, ions and neutral energetic particles from flares and/or CMEs can be detected directly. Here we list some of the diagnostics for the energetic particles, along with some of the context observations that are important for understanding the physical parameters in the region where the acceleration occurs. Detailed reviews of high energy observations of flares are contained in Emslie et al. (2011), including an overview of observations (Fletcher et al. 2007) and discussion of the physics and interpretation of emission by electrons (Holman et al. 2011) and ions (Vilmer et al. 2011). Radio observations are discussed in White et al. (2011) in that volume and in a separate review by Pick and Vilmer (2008).

#### 3.1 Energetic Electrons

Energetic electrons produce bremsstrahlung radiation when they encounter other particles (see Kontar et al. 2011 for a review). Large flares accelerate electrons to hundreds of MeV. A recent review is given by Holman et al. (2011). In principle, the spectrum of the bremsstrahlung-emitting electrons can be obtained from the observed photon spectrum in a model-independent way (Johns and Lin 1992; Kontar et al. 2007; Piana et al. 2007; Petrosian and Chen 2010), but this requires high statistical accuracy of the observation. For ‘thick target,’ meaning that each electron loses all its energy by Coulomb collisions, gradually slowing down and producing softer photons, and in the idealized situation where the acceleration can be considered separate (e.g., in the tenuous corona) from loss to collisions (in the dense chromosphere and photosphere) the spectrum of the accelerated electrons can be inferred. A complete treatment includes electron-electron bremsstrahlung, relativistic cross sections, reflection of X-rays from the solar surface, radiative recombination radiation (Haug 1997; Kontar et al. 2007, 2011; Brown et al. 2010), and possibly inverse Compton scattering (Chen and Bastian 2011). From hard X-ray observations the inferred electron spectrum is typically a broken power law, with a break at tens of keV. This break could be attributed to non-uniform ionization in the thick target region, to effects of the return current on the transport between the acceleration region and the chromosphere, or to the acceleration process itself (Holman et al. 2011). The inferred particle spectral indices  $\gamma$ , where  $N(E) \propto E^{-\gamma}$ , range from  $\gamma$  near 2 to  $\gamma$  above 6 (Dulk et al. 1992; Kiplinger and Winglee 1992). On the other hand, when photon spectra are obtained over a broad band extending to gamma-ray range one sees a flattening at around several 100 keV and a cutoff around several tens of MeV. This is especially true for large electron-dominated flares (Trottet et al. 1998) and in recent June 12, 2010 flare observed by *Fermi* (Ackermann et al. 2012). These features cannot be due to transport effects and must be a reflection of the acceleration mechanism (Petrosian et al. 1994). Therefore, these can be used to determine the acceleration mechanism parameters (Park et al. 1997).

**Fig. 1** Example of thermal (*red*) and non-thermal (*magenta*) components in a hard X-ray spectrum, along with gamma ray emission in *blue* (Lin 2011). Note the thermal Fe  $K\alpha$  line near 6.5 keV and the narrow and broad gamma ray lines



In general, the hard X-ray spectrum of a flare includes both thermal and non-thermal continua, along with emission lines such as Fe  $K\alpha$ . In principle, thermal and non-thermal components can be separated by spectral fitting, as suggested in Fig. 1. In practice, the low energy cutoff of the non-thermal component, and therefore the total non-thermal energy, are difficult to determine unambiguously (Guo et al. 2011).

Emission from the footpoints and the loop tops can sometimes be separated in images from the Yohkoh and RHESSI satellites, especially for limb flares, as shown in Fig. 2. The footpoint X-rays are interpreted as thick target emission because of the high density in the chromosphere, while loop top X-rays are taken to be thin target because of the long mean free paths at coronal densities. However, loop densities can be quite high, and trapping of particles can further increase the path enough to produce emission that is intermediate between the thin and thick target limits (Veronig and Brown 2004).

Energetic electrons are also observed at radio and sub-mm wavelengths through gyrosynchrotron emission and conversion of Langmuir waves into electromagnetic waves. Their manifestations include subsecond bursts at sub-mm wavelengths (Kaufmann et al. 2009), long-lasting type IV bursts from electrons trapped in stationary or expanding magnetic structures and type III bursts from beams of electrons that propagate rapidly up from the flare (Pick and Vilmer 2008; White et al. 2011). In principle, by comparing hard X-ray and gyrosynchrotron emission from a flare, one can determine the magnetic field in the emitting region. However, the radio and X-ray spectra sometimes indicate incompatible spectral indices. This may be caused by the different electron energies that dominate in the two wavelength regimes, by anisotropy of the particle distribution, or by optical depth effects in the radio (White et al. 2011).

### 3.2 Energetic Ions

Large flares can accelerate ions up to  $\gtrsim 10$  GeV. Energetic ions can be observed by means of the gamma-ray line and pion decay continuum gamma-ray emission that they produce upon impact on the chromosphere, and by way of neutrons and energetic ions and atoms SEP that reach the Earth.

Gamma ray lines are produced by nuclear de-excitation and neutron capture, and by annihilation of positrons produced by ions in the 1–100 MeV/nucleon range, and more energetic

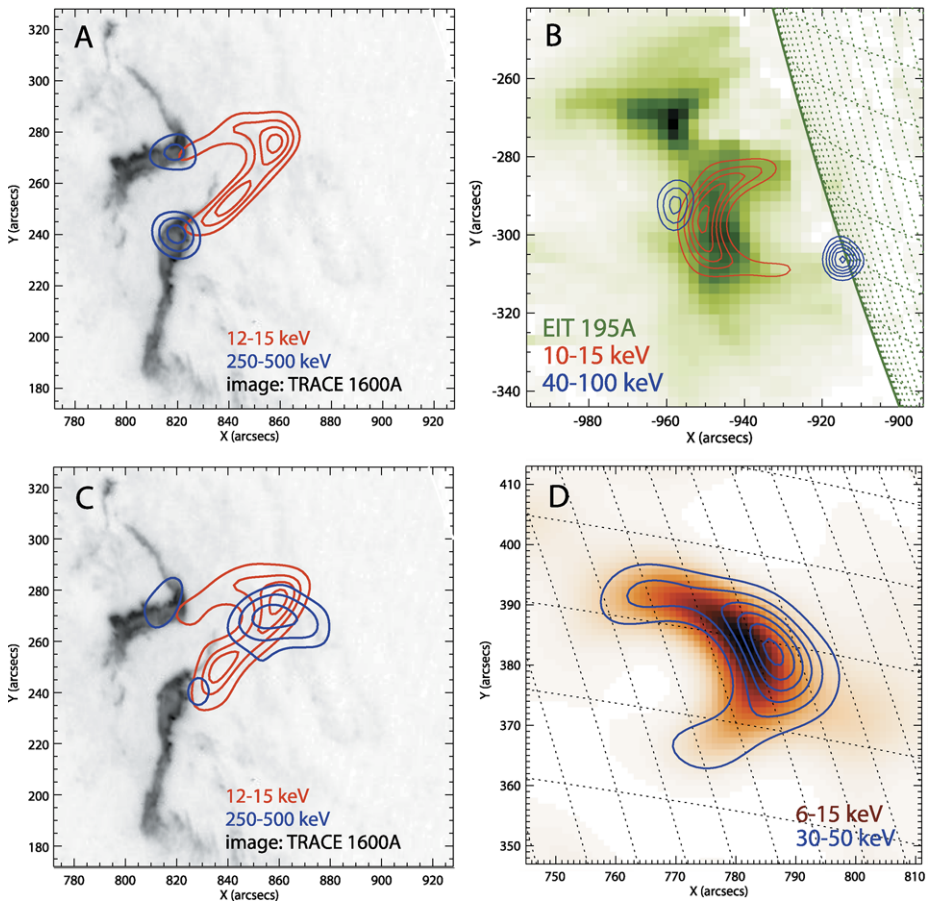


**Fig. 2** Examples of HXR imaging of flares from RHESSI. (A) Simple single loop flare with non-thermal emission from chromospheric footpoints (*blue*) and thermal emission from the flare loop (*red*). (B) Flare with an additional non-thermal source above the flare loop similar to the Masuda flare (from Ishikawa et al. 2011). (C) Same as event as shown in (A), but during the decay of the hard X-ray emission revealing a coronal source seen up to 1 MeV (from Krucker et al. 2008). (D) A rare event with non-thermal emission from the flare loop itself without emission from the footpoints (from Veronig and Brown 2004)

ions can produce a continuum through decay of pions generated in nuclear collisions. The nuclear emission lines provide information about the spectrum of energetic particles, the acceleration timescale, and the elemental abundances of both the chromosphere and the accelerated ions. The ratio of broad and narrow components of the positron annihilation line and the width of the narrow component indicate the temperature in the region where the energetic particles deposit their energy (Share et al. 2003). Measurements of neutrons in space or on the ground, along with gamma rays from pion decay, constrain the higher energy part of the spectrum. Models of the transport and interaction are used to interpret the observed spectra in terms of accelerated particle spectrum and number (Murphy et al. 2007). Such a model for the X4.8 flare on 2002 July 23 is shown in Fig. 3.

The RHESSI satellite provides both images of the gamma ray emission and profiles of nuclear lines and positron annihilation lines. A recent review is given by Vilmer et al.

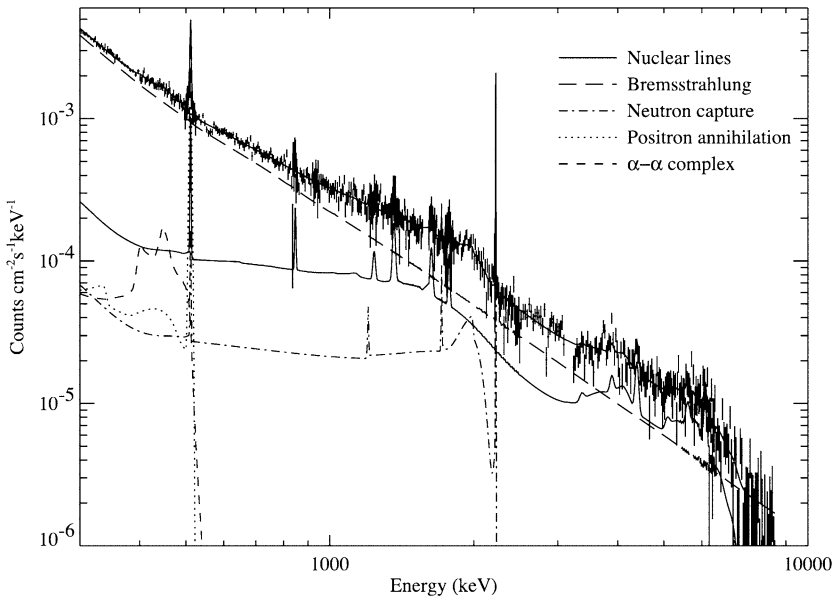


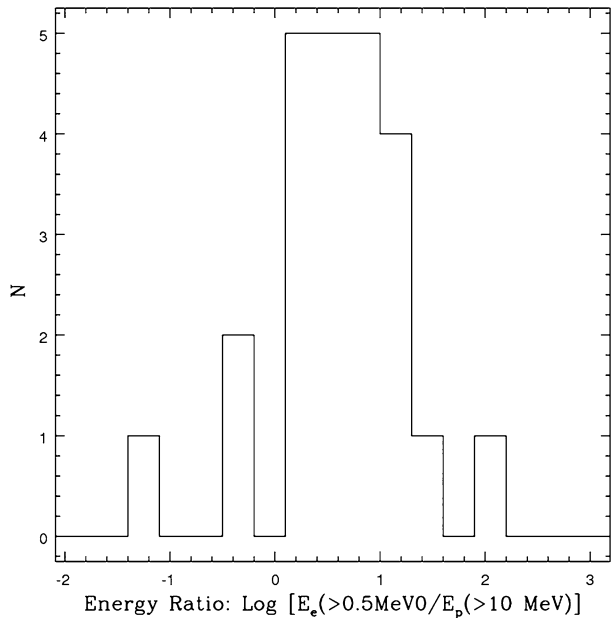
**Fig. 3** RHESSI gamma-ray spectrum from the 2002 July 23 event showing the contributions of different line and continuum processes to the total (Lin et al. 2003)

(2011). Most recently, energetic neutral atoms produced by charge transfer between energetic ions and coronal ions have been reported by Mewaldt et al. (2009). Shih et al. (2009) find a roughly linear correlation between gamma rays from neutron capture and very hard,  $>0.3$  MeV, X-rays from electron bremsstrahlung, which implies a strong correlation between electron and proton acceleration at very high energies, although with large dispersion (Fig. 4).

Observed spectra and isotopic abundance ratios of SEPs are another signature of acceleration in flares. SEPs show varied spectra and a large range of isotopic enhancement particularly for  $^3\text{He}$  and ions heavier than CNO. In the case of He the observed  $^3\text{He}/^4\text{He}$  fluence ratio extends from the photospheric value to several thousand times higher, with more enriched events being weaker and more impulsive (Mason et al. 2002a, 2002b; Reames et al. 1994, 1997; Ho et al. 2005). As discussed below, SEPs may undergo acceleration both at the coronal acceleration site (impulsive flares) and again at the CME shock (gradual flares).

A potentially valuable signature of energetic ion precipitation in the chromosphere would be broad, red-shifted wings on the  $\text{Ly}\alpha$  or  $\text{He II } \lambda 30.4$  nm lines (Orrall and Zirker 1976; Peter et al. 1990). These could arise through recombination or charge transfer onto fast ions, and through collisional excitation of the recombined ions. However, such wings have not yet been detected (Hudson et al. 2012). Likewise, wings should appear on some soft X-ray lines, but none have yet been reported (Raymond 2012). Such signatures would be valuable indicators of the amount of energy carried by ions below a few MeV, which would dominate the ion energy if the spectrum is steep, but which cannot be observed by means of gamma-rays.

**Fig. 4** Using the ratio of fluxes (in units of particles  $\text{cm}^{-2} \text{s}^{-1} \text{MeV}^{-1}$ ) of electrons  $J_e$  (0.5 MeV) and protons  $J_p$  (10 MeV) obtained by Shih et al. (2009) we estimate the electron to proton energy ratio  $R = (0.5/10)^2(J_e/J_p)$ . The histogram shows the distribution of  $R$



### 3.3 Indirect and Context Observations

A vast range of observations at other wavelengths provides necessary information about flare structure where acceleration occurs. Magnetograph measurements are used to compute the structure of the coronal magnetic field that leads to an eruption. White light and UV and EUV imaging show the footpoints, and footpoint motion can be used to infer the reconnection rate in the corona. The combination of footpoint motion with field strength gives the electric field in the reconnecting plasma (Qiu et al. 2002). X-ray and UV measurements of Doppler shifts reveal the response of chromospheric plasma to sudden heating, in some cases suggesting evaporation of chromospheric plasma to fill the flare loops.

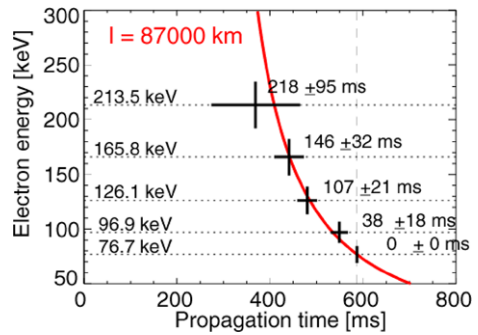
There is also a growing number of observations that constrain the physical parameters in the current sheets associated with flares and CMEs. X-ray observations, especially of events whose bright footpoint emission is occulted by the solar limb, show the X-point position (Sui and Holman 2003; Liu et al. 2009). Soft X-ray and EUV images show current sheet structure and both upward and downward motions of contracting loops (McKenzie and Savage 2009; Savage et al. 2010) and reconnection speeds (Yokoyama et al. 2001). UV spectra are used to determine temperatures, densities, flow speed and turbulent velocities inside the current sheets (Innes et al. 2003; Ciaravella and Raymond 2008; Bemporad 2008).

## 4 Particle Acceleration in the Standard Picture

In the standard picture, particle acceleration occurs in the reconnection region, generally taken to be the current sheet. The reconnection rate must be fast, with an Alfvén Mach number of order 0.05 to 0.1, to explain the rapid rise. This may be due to collisionless effects, a tearing-type instability, or Petschek-type slow mode shocks or other discontinuities. Hard X-ray observations of above the looptop sources put the acceleration region at



**Fig. 5** Time of flight analysis of hard X-ray emission as a function of time shows that more energetic electrons reach the chromosphere sooner, as expected for propagation from the top of a coronal loop (adapted from Aschwanden et al. 1996)



about 20–30 Mm above the photosphere (Masuda et al. 2000; Petrosian and Donaghy 1999; Krucker et al. 2011b; Ishikawa et al. 2011). Most of the energetic particles precipitate to the chromosphere. Key constraints on the acceleration mechanism come from the timing of the emission, the location, the spectrum and the particle composition. In addition, important constraints on the physical parameters of the reconnection current sheet are available from indirect measurements.

#### 4.1 Timing

The brightness of the flare as a whole increases with a time scale of the order of 100 seconds, and much of that is due to successive brightening of different magnetic flux tubes. Individual footpoints turn on at 1700 Å within the 4 to 8 second cadence of TRACE (Hudson et al. 2006). Coincident with the hard X-ray and optical/UV rise, UV emission lines brighten and exhibit Doppler shifts up to about 100 km/s, perhaps indicating shock waves moving downward and chromospheric evaporation flows moving upward (Milligan and Dennis 2009; Raymond et al. 2007). CME acceleration also occurs at about the same time with a similar profile in time (Zhang et al. 2004; Temmer et al. 2010). Pairs of footpoints brighten at the same time to within a few tenths of a second, which is expected if electrons are accelerated in the corona, but potentially a problem for acceleration in the chromosphere (Sakao et al. 1996).

Within the impulsive phase, fine structure is seen with time scales of order 0.1 seconds in both X-rays and radio (Dmitriev et al. 2006; Kaufmann et al. 2009). These pulses are consistent with direct transport of electrons from the corona into the chromosphere, in that the lower energy electrons should be delayed relative to the high energy electrons by the loop length divided by the velocity. The expected time of flight is 0.01 to 0.1 seconds, in agreement with measurements from CGRO. Figure 5, adapted from Aschwanden et al. (1996), shows an example of the time delay versus energy. The fine structure can be interpreted as injection of electrons into a magnetic loop and the rapid precipitation of those within the loss cone defined by the expansion factor of the magnetic flux tube between the chromosphere and corona. These short time scales are usually interpreted as requiring acceleration time scales below 0.1 seconds.

The electrons not originally in the loss cone will be trapped in coronal magnetic flux tubes before they precipitate into the chromosphere. Magnetic mirroring confines the electrons until collisions or pitch angle diffusion brings them into the loss cone, and this can lead to delays as large as 10 seconds. Dauphin and Vilmer (2007) interpret the 12 second delay between hard X-rays and gamma rays in the 23 July 2003 event in terms of different trapping parameters for the coronal magnetic field loops that contain the electrons and the

ions. Krucker et al. (2008) showed that the observations are consistent with flare-accelerated electrons at higher energies being trapped longer than low energy ones. Direct observation of a coronal HXR source and simultaneously one of the associated footpoint sources (Fig. 3B) are consistent with trapping and precipitation (Ishikawa et al. 2011). Consequently, hard-X-ray and even gamma-ray emission from the trapped electrons can be seen during the decline of the hard X-ray burst (see Fig. 3C).

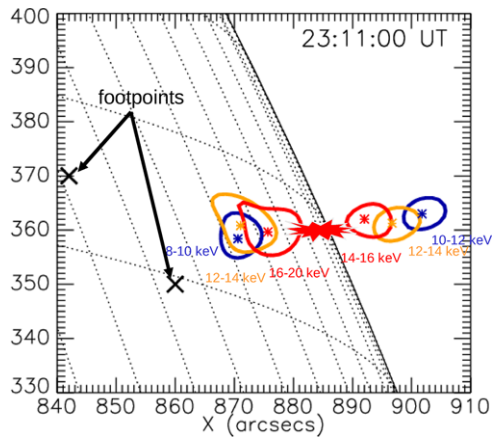
## 4.2 Location

*Looptop and above the looptop hard X-ray sources:* A strong piece of evidence for acceleration in the corona is provided by observations of hard X-ray emission above the soft X-ray loops, apparently from the acceleration region. The best-known case is the Masuda flare (Masuda et al. 2004). Analysis of other limb flares observed by Yohkoh shows that hard X-ray looptop sources are more the rule than the exception (Petrosian et al. 2002), and RHESSI data have confirmed this (Lin et al. 2003). Partially disk-occulted observations clearly establish that coronal hard X-ray emission is present in all flares (e.g., Krucker and Lin 2002). With high spectral resolution measurements of the hard X-ray coronal source above the soft X-ray looptops in a limb-occulted flare on 2007 December 31, Krucker et al. (2010) placed upper limits on hot thermal plasma and showed that the spatially coincident hard X-ray and microwave emission from this source are consistent with bremsstrahlung and gyrosynchrotron emission, respectively, from a single population of suprathermal particles. The HXR source dimensions are  $\sim 29$  Mm long by  $\sim 6$  Mm wide for a volume of  $\sim 8 \times 10^{26} \text{ cm}^{-3}$  (assuming depth equal to width), and the density of non-thermal electrons is  $\sim 2 \times 10^9 \text{ cm}^{-3}$  for a total of  $\sim 2 \times 10^{36}$  electrons above 16 keV. The number of suprathermal particles is comparable to or greater than that of plasma in the emitting region, and it would heat the plasma to tens of keV within seconds. This indicates that the entire coronal plasma within the HXR source has been energized in a bulk acceleration process. The magnetic field in this source was estimated from the turnover in the microwave spectrum to be  $\sim 30$  to 50 G; this implies a magnetic field energy density comparable to that of the accelerated electrons above 16 keV, e.g., a plasma  $\beta \simeq 1$ . Before the flare, no HXR were detected from this source, so the pre-flare  $\beta$  is likely to be very low,  $\sim 0.01$ . These observations appear to be consistent with the scenario proposed by Drake et al. (2006a, 2006b), that magnetic reconnection in narrow current layers should lead to multiple secondary magnetic islands; in three dimensions, these should be volume filling. As the elongated islands contract to a more potential configuration, electrons circulating rapidly within the islands will gain energy by reflecting off the ends of the islands that are traveling inward at the Alfvén speed. The contraction stops when  $\beta \simeq 1$ , thus essentially accelerating bulk electrons with high efficiency.

In the case shown in Fig. 6, X-rays appear to originate above and below an X-line, and the softening of the spectrum with distance from the central point strongly suggests energy loss with distance from the energy release and particle acceleration region (Sui and Holman 2003; Liu et al. 2008; Chen and Petrosian 2012). In addition, the detection of non-thermal hard X-rays and superhot (temperature  $> 30$  MK) thermal plasma above the normal flare soft X-ray loops prior to the impulsive phase of the 2002 July 23 flare (Caspi and Lin 2010) also indicate that the energy release/particle acceleration site is high in the corona. Occasionally, non-thermal hard X-ray emission is observed at the top of the flare soft x-ray loops. The sizes of the looptop sources are typically 10–18" (Xu et al. 2008).

Observations of hard X-rays from looptop sources place stringent demands on the numbers and spectra of accelerated particles (e.g., Battaglia and Benz 2008). Petrosian and Chen

**Fig. 6** Centroids of emission at different energies showing the energy loss with distance away from the acceleration point during a flare on 2002 April 15 (adapted from Sui and Holman 2003)



(2010) obtained energetic electron flux images directly from the RHESSI hard X-ray measurements, using a powerful new inversion method (Piana et al. 2007). Their results are consistent with the electrons being accelerated (in their model through turbulence) at or near the looptop region, then escaping downward to the dense footpoint regions where they produce thick target X-ray emission. For a very powerful flare that was 40 degrees behind the limb, hard X-ray emission was detected from a source 150,000 km in extent, that was expanding and moving upward at 750 km/s behind a fast CME. The energetic  $>10$  keV electrons were  $\sim 10\%$  of the total plasma density in the source. Similar hard X-ray emission has been detected from most fast CMEs from behind the limb. Gamma-ray continuum observations above 200 keV for three powerful flares show that emission from the top of the coronal loop dominates during the decay phase, with hard spectra that imply that the bulk of the gamma-ray emitting electrons are above 1 MeV (Krucker et al. 2008). Chen and Bastian (2011) have suggested that at least in some cases, gamma-rays could be produced by inverse Compton scattering of photospheric photons by relativistic electrons or by scattering of EUV photons from the flare by mildly relativistic electrons. This may reduce the required number of accelerated electrons, but whether one can build a complete flare emission picture on this basis remains to be seen.

*Footpoints:* One of the major surprises from RHESSI observations was a spatial offset between hard X-ray and gamma ray footpoints in the few imaged gamma-ray flares. Figure 7 shows the hard X-ray and gamma-ray footpoints of the 28 October 2003 flare studied by Hurford et al. (2006) superposed on a TRACE 195 Å image. Images in the neutron capture line at 2.223 MeV show that the gamma-ray footpoints lie near the footpoints dominated by electrons, but are in some cases displaced by as much as  $20''$  (Hurford et al. 2006). This implies either that electrons and ions are accelerated on different magnetic field lines, or that they propagate differently along the flux tubes.

Footpoint motion and surface magnetic field can be combined to infer the reconnection rate in the corona. Krucker et al. (2005) followed the HXR footpoint motion in a flare through a series of intensity peaks and dips, and they compared the estimated rate of energy release to the rate of energy deposition in the chromosphere estimated from the hard X-ray flux and spectral index (with an assumed low energy cutoff). As shown in Fig. 8, the correlation is remarkably good for some time intervals, while no correlation is observed for others.

**Fig. 7** Hard X-ray and gamma-ray contours of the 28 October 2003 flare superposed on a TRACE 195 Å image

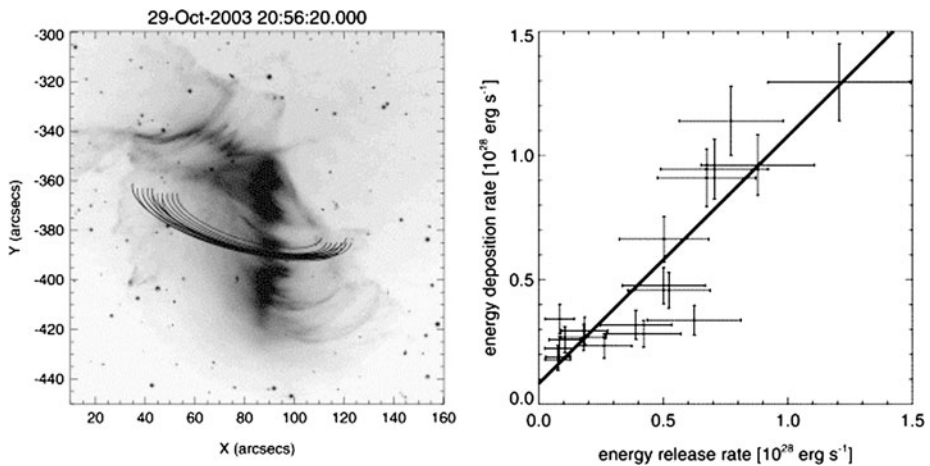
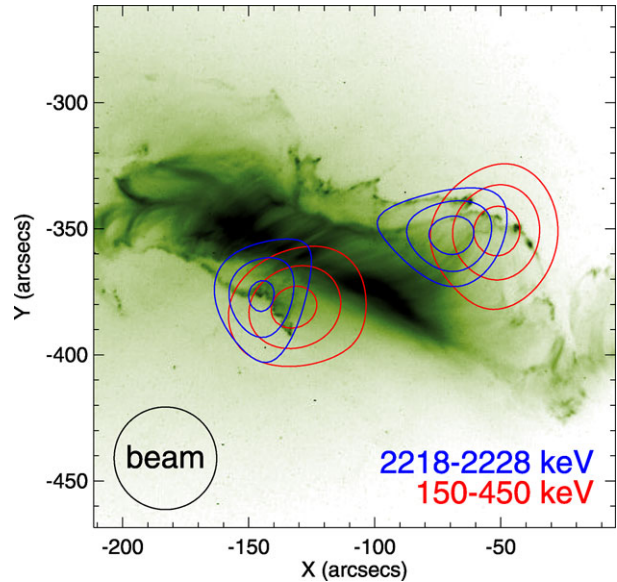


**Fig. 8** The *left panel* shows a TRACE 195 Å image with superposed *semicircles* that connect pairs of simultaneously brightening footpoints. The *right panel* shows the correlation between energy dissipation rate inferred from footpoint motions and the power deposited at the footpoints as inferred from the hard X-ray spectra (Krucker et al. 2005)

#### 4.3 Spectrum

The spectrum of energetic electrons inferred from the hard X-ray spectrum is a power law or a double power law with a break, often sharp (Conway et al. 2003), at tens of keV energy to  $>100$  keV for large flares. In the standard picture, thick target emission from the footpoints produces a photon spectrum flatter than the particle spectrum by 1, while thin target emission at the top of the loop produces a photon spectrum steeper than the particle spectrum by 1. Thus, in the simplest picture one expects a difference of 2 between footpoint and looptop

hard X-ray spectra. While Battaglia and Benz (2006) found steeper spectra from coronal sources than from footpoints, the difference in spectral indices ranged from 0.59 to 3.68 among five flares analyzed. Thus, caution is needed when interpreting X-ray spectra in terms of particle spectra.

A low energy cutoff or spectral break must be present, both to avoid a divergence at low energy and because the electrons at modest energies rapidly thermalize. It is difficult to determine the low energy cutoff, because it is masked by thermal emission, but its value is crucial to determination of the total number and energy of the accelerated particles (Holman et al. 2011). Only upper limits to the low energy cutoff can be determined. Contributions from photons Compton scattered in the photosphere or low chromosphere, anisotropy in the electron beam and bremsstrahlung differential cross section (Kontar et al. 2008), variations in the ionization state of the target region (Kontar et al. 2003), or energy losses related to the return current (Battaglia and Benz 2008) can all affect determination of the low energy cutoff, so few reliable determinations of the cutoff energy are available. Upper limits to the cutoff energy are typically 15–45 keV (Holman et al. 2011). A statistical study by Kontar et al. (2008) concluded that the low energy cutoff is below 12 keV.

The spectrum also evolves with time. The most common pattern in the impulsive phase is the so-called *soft-hard-soft* (SHS) pattern, in which the hard X-rays become harder during the rise to peak intensity, then soften during the decline of the impulsive phase (Grigis and Benz 2004). A *soft-hard-harder* (SHH) pattern is correlated with SEP events in flares magnetically connected to Earth (Kiplinger 1995; Grayson et al. 2009). Evidence for a *hard-soft-hard* (HSH) pattern has been reported above 50 keV in spikes seen in a flare (Shao and Huang 2009). The spectral evolution is determined by the interplay of acceleration efficiency, escape from the acceleration region, and propagation to the target region. Observation of SHS spectral evolution in the coronal source indicates that the pattern is not caused by transport effects in the loop, but by the acceleration process (Grigis and Benz 2004).

In some large flares the observed photon spectrum extends to 100's of MeV. Some of these are electron-dominated flares, indicating acceleration of electrons to 100's of MeV (Petrosian et al. 1994). Such flares show additional deviations from a simple power law, providing good constraints on the transport and acceleration of electrons (Petrosian et al. 1994). The Fermi gamma ray telescope has begun to observe more gamma ray flares, several of which show emission to several 100 MeV. The first Fermi flare (2011, June 12) shows the same features as the electron-dominated flares, but also gamma-ray lines and a higher energy (>100 MeV) continuum indicating acceleration of protons and other ions to the GeV range (Ackermann et al. 2012). The spectrum of energetic ions is more difficult to determine. In principle, comparison of nuclear emission lines with different excitation thresholds should yield a spectral index, but in practice uncertainties in elemental abundances and in the  $\alpha/p$  ratio of the accelerated particles can make the results ambiguous, and proton and alpha particle spectra may differ (Vilmer et al. 2011). However, tighter constraints can be obtained when line emission is accompanied by pion decay continuum radiation. Fermi observations mentioned above (Ackermann et al. 2012) show the possible presence of pion decay  $\gamma$ -rays, which can constrain the accelerated proton spectra and pitch angle distribution (Murphy et al. 1987, 2007).

The scaling of non-thermal particle properties with flare size is an important consideration for theories of particle acceleration. For instance, a small physical scale should limit the trapping time and impede acceleration to very high energy. In general, a power law distribution of the number of flares versus flare energy seems to hold from microflares through the most powerful events that have been observed, but exact determinations are limited by unavoidable bias effects (Hannah et al. 2011). Small events typically resemble more energetic flares in having an impulsive non-thermal phase followed by a gradual thermal phase.

They differ in that the small events have softer non-thermal spectra and lower temperatures (Hannah et al. 2011). Type III bursts indicate that microflares sometimes have access to open field lines, and EUV and X-ray jets seem to be more prominent in microflares, suggesting that some of the energy release occurs on open field lines (Strong et al. 1992; Hannah et al. 2011).

#### 4.4 Energetics

Relatively few determinations of the global energetics of solar eruptions are available because that requires data on CMEs and radiation covering the full range of wavelengths, along with an accurate model of the magnetic field structure. In addition, energy is rapidly exchanged between different forms, such as kinetic and thermal energy, which makes the accounting difficult. Thermal emission and non-thermal electron and proton energies are comparable, indicating efficient conversion of non-thermal to thermal energy (Holman et al. 2003; Saint-Hilaire and Benz 2005). Much of the radiated energy emerges at UV and optical wavelengths. Woods et al. (2004) used data from the *SORCE* satellite to measure the total irradiance from a large flare. Emslie et al. (2005) estimated the magnetic energies, energies in accelerated electrons, protons and thermal plasma, radiant energies and CME energies for two large flares, using the Woods et al result for the ratio of total radiated energy to GOES X-rays, and they found comparable energies for the different components. Raymond et al. (2007) used UVCS observations to determine the transition region emission during the impulsive phases of five flares in order to estimate conductive losses. Woods et al. (2006) report the total solar irradiance from several large flares and the correlation between GOES X-rays and EUV emission for a larger number of flares based on *SORCE* and *TIMED* measurements. Observations with the *EVE* instrument on *SDO* (Hock et al. 2010) with 10 second cadence will greatly help to establish the complete budget of radiation in flares. The non-radiative parts of the energy budget include the kinetic energy of CMEs (Vourlidas et al. 2010) and the heating of CME plasma (Murphy et al. 2011). One of the most difficult aspects of the problem is the magnetic free energy, which has been recently investigated for four flares by Kazachenko et al. (2011).

#### 4.5 Composition

While there is a good correlation between the intensities of hard X-rays and gamma-rays produced by electrons and ions, respectively, it is relatively difficult to determine the ratios of the numbers and total energies of electrons and ions. Emslie et al. (2005) found comparable ion and electron energies in two X-class events, but the uncertainties were substantial, mostly due to the unknown lower energy cutoffs for electrons and especially ions (gamma-ray line measurements only sample ions above a few MeV).

The composition of the accelerated ions can be measured from the gamma ray spectrum. Emission from chromospheric ions excited by impinging energetic ions produces narrow emission lines, while emission from the energetic ions is quite broad, with Doppler widths as large as 20 % of the line energy. Because there are many lines, the broad lines blend together into a quasi-continuum (Murphy et al. 1990), but nuclear excitation models can be used to extract relative elemental abundances. Murphy et al. (1991) found in one event that the abundances of the low First Ionization Potential (FIP) elements Mg, Si and Fe relative to C were similar to the coronal abundance ratios rather than photospheric abundances. The O/C abundance ratio matched both photospheric and coronal values, while He/C was 2 or 3 times smaller than the photospheric and coronal ratios. The  $^3\text{He}/^4\text{He}$  ratio was uncertain, but appeared to be enormously enhanced compared to normal values. It is similar to the class of impulsive electron- $^3\text{He}$ -rich SEP events.

#### 4.6 Flares and SEP Events Observed in the Interplanetary Medium

In the interplanetary medium, flare-accelerated particles are distinguished from those accelerated by large scale shocks driven by CMEs primarily by their arrival time in the so-called ‘impulsive’ vs. ‘gradual’ picture of Reames (1999), though the real situation is more complex (Cane et al. 2006; Krucker et al. 1999). Impulsive SEP events are the most common solar particle acceleration observed in the IPM, with up to  $\sim 10^4$  events/year (after correction for events hidden by high background fluxes; Wang et al. 2011) over the whole sun near maximum, detected primarily in  $\sim 1$ – $100$  keV electrons (Lin 1985; Wang et al. 2012a). They are accompanied by low fluxes (often below detection threshold) of  $\sim 0.01$ – $1$  MeV/nucleon ions (thus, high  $e/p$  ratios similar to  $\gamma$ -ray flares), with large enhancements of  $^3\text{He}$  and ultra-heavy ( $\sim 100$ – $200$  amu) ions, Fe enhancement of  $\sim 10$  (Mason 2007), and high charge states (e.g.,  $\text{Fe}^{+20}$ ) indicating high temperatures and/or stripping in the acceleration process (Möbius et al. 2003). Only  $\sim 25$  % of these events, however, have associated SXR/H $\alpha$  flares reported by GOES, but all (99 %) have low frequency ( $\lesssim 10$  MHz) type III radio bursts (Wang et al. 2012a). In most (80 %) of the events, the onsets of the  $>20$  keV electrons at 1 AU are delayed by  $\sim 10$ – $30$  minutes relative to the type III burst and lower energy electrons (Krucker et al. 1999; Haggerty and Roelof 2002).

Various models are used to interpret the large isotopic enhancements. In the case of the  $^3\text{He}/^4\text{He}$  ratio, the charge to mass ratio ( $2/3$  vs.  $1/2$ ) has been thought to play a role (Fisk 1978; Ibragimov and Kocharov 1977); More recently Liu et al. (2004) and Liu et al. (2006) show that the stochastic acceleration by electromagnetic waves (not the electrostatic waves considered earlier) can account for the large observed enhancements as well as the distribution of enhancements observed by Ho et al. (2005) mentioned above (Petrosian et al. 2009).

In the hard X-ray energy range, the electron energy spectra are typically double-power-law with a downward break at a few tens of keV, very similar to the non-thermal HXR spectra observed for flares. In impulsive events, Krucker et al. (2009) found that the power-law index,  $\delta_e$ , for  $>50$  keV electrons observed in the IPM is linearly correlated with the index,  $\gamma_x$ , for the flare HXRs,  $\delta_e = \gamma_x$ ; clearly different from  $\delta_e + 1 = \gamma_x$  expected for a single acceleration high in the corona that produces both the electrons freely escaping to the Interplanetary Medium (IPM) and those losing all their energy to collisions in the solar atmosphere generating thick target HXR emission. The number of escaping electrons is only  $\sim 0.1$  % of the number needed to produce the HXRs. This suggests that the electrons (and protons and other ions) may be initially accelerated by interchange magnetic reconnection high in the corona, with those escaping on the open field lines producing the impulsive emission and the type III burst in the IPM and the SEPs, while those trapped on closed field lines are further accelerated as the field lines contract and become more potential. HXR imaging shows evidence for interchange reconnection, where an open field line reconnects with a closed loop (Heyvaerts 1975) in many of these events (Krucker et al. 2011b; Glesener et al. 2012). Impulsive SEP events also appear to be associated with coronal jets (Wang et al. 2006) near coronal holes, and/or with fast narrow CMEs (Kahler 2007; Wang et al. 2012b) that could further accelerate the electrons to produce the delayed onsets for  $>20$  keV electrons seen in the most impulsive events.

The most powerful ion accelerators (sometimes reaching 10–100 GeV energies) in the solar system are large gradual SEP events (discussed in the accompanying reviews by Lee et al. 2012), that are associated with fast wide CMEs. These CMEs are typically accompanied by a large flare, and the acceleration vs. time profile of the CME itself is found to be closely

correlated with the flare energy release as measured by the HXR flux vs. time profile, consistent with standard models for large solar eruptions with magnetic reconnection occurring in a current sheet behind the CME.

#### 4.7 Current Sheet Properties

Popular models for the reconnection current sheet are the Petschek and the turbulent models. Acceleration mechanisms include turbulence, DC electric fields and shock waves.

In Petschek reconnection, there is a small diffusion region where MHD breaks down and strong electric fields are present. Slow mode shock waves or similar structures extend out from the diffusion region at modest angles to the symmetry line. The diffusion region itself is expected to be very small, of order tens of km, and it contains far too little magnetic energy to account for the flare and far too few electrons to account for observed hard X-rays. The reconnection process, however, changes the topology of the magnetic field from anti-parallel fields to loops or islands or turbulence that are highly elongated; then the bulk of the energy in the magnetic field can be released as the loops/islands/turbulence relax to more potential configuration. Therefore, most of the magnetic energy dissipation must occur in the slow mode shocks and most of the acceleration must happen in the exhaust region. Possibilities include acceleration at the slow mode shocks, acceleration at a fast mode shock where the Petschek outflow encounters stationary loops (Aurass and Mann 2004), acceleration by stochastic turbulence (Shibata et al. 1995; Liu et al. 2008), acceleration in contracting magnetic islands (Drake et al. 2006a) and initial acceleration of heavy ions as they are picked up in the reconnection exhaust (Drake et al. 2006b).

Turbulent reconnection could occur over a large volume (Lazarian and Vishniac 1999), though it consists at any moment of a large number of tiny reconnection sites. Particle acceleration could occur by a second order Fermi interaction between particles and turbulence, such as that proposed by Miller (1997), by interaction with large scale electric fields (Litvinenko 2006) or small scale fields (Vlahos et al. 2004) or by a first order process of interaction with small reconnection sites in a turbulent reconnection current sheet (Lazarian et al. 2011).

Observations of current sheets cannot yet discriminate among the possibilities, but they provide some constraints on current sheet parameters. A fine example of a current sheet is shown in Fig. 9. In this TRACE image in the 195 Å band, the bright loops are interpreted as emission in the Fe XII lines from gas that has cooled below 2 MK, while the diffuse structure above the loops is attributed to Fe XXIV emission from a fan-shaped sheet of 15 MK gas. The structure of the Fe XXIV sheet includes “tadpoles” which are dark, sinuous, roughly vertical features that work their way downwards at moderate speeds (Gallagher et al. 2002). They are neither low temperature nor absorption features, but rather low density voids (Innes et al. 2003). These features have been interpreted as shrinking reconnected flux tubes (Longcope and Guidoni 2011). In the magnetosphere, this process is known as “dipolarization”, and it can further energize the particles. The hot supra-arcade structures can now be observed with AIA. The 3 Nov. 2010 event discussed by Reeves and Golub (2011) and Cheng et al. (2011) demonstrates how well such a structure shows up in the 94 Å and 131 Å bands dominated by plasma in the 6–15 MK range, and it shows how the structure associated with the current sheet can be connected to the evolution of the magnetic flux rope.

UV spectral observations of the 2002 April 21 current sheet with the SUMER instrument on SOHO revealed strong emission in a forbidden line of Fe XXI (Innes et al. 2003). The line was 1000 km/s broad and somewhat blue-shifted. Innes et al. (2003) attribute the emission to the interaction of downflowing plasma with the stationary arcade of bright loops seen in



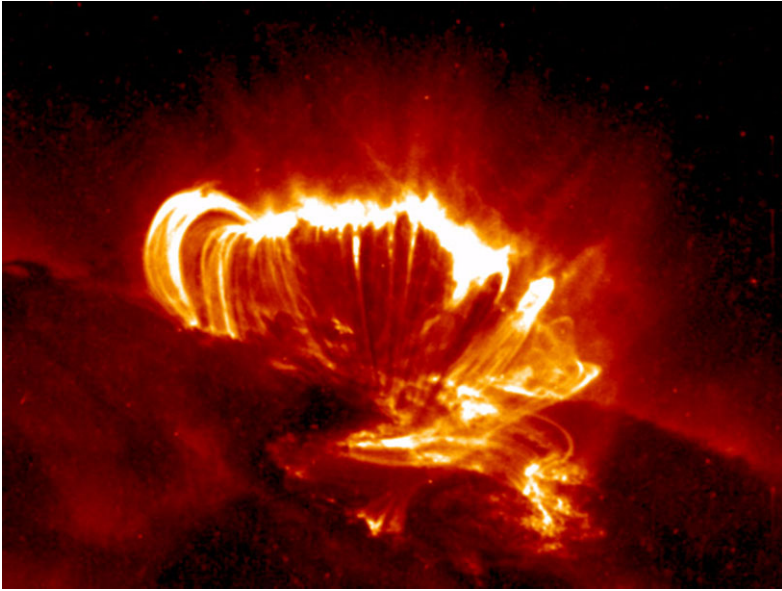


**Fig. 9** Image of a solar flare on 21 April, 2002 from the TRACE satellite. The narrow EUV band at 195 Å shows both million K plasma in the bright loops and 15 MK in the diffuse structure above the loops. (Image courtesy of NASA)

Fe XII. The Fe XXI emission line indicates thermal plasma at around 15 MK, while the RHESSI hard X-ray emission reported by Sui and Holman (2003) in the 15 April 2002 flare arises from non-thermal electrons.

Current sheets have also been observed at larger heights. In the standard picture, these current sheets connect the flare to the core of the CME, and the upward reconnection outflows help to accelerate the CME. Upward propagating energetic particles might heat the CME core (Krucker et al. 2007), but the heating mechanism is not yet known (Murphy et al. 2011). Yokoyama et al. (2001) used a series of EIT images and Lin et al. (2003) used UVCS spectra to track the inflow into post-eruption current sheets to determine the reconnection rates, with estimated Alfvén Mach number of 0.01 to 0.1. UVCS spectra have shown current sheet emission from 2–9 MK plasma (Ciaravella et al. 2002; Ko et al. 2003; Bemporad et al. 2006; Ciaravella and Raymond 2008). As the current sheet fades over time scales of hours, the plasma cools. Densities at 1.7  $R_{\odot}$  are around  $7 \times 10^7 \text{ cm}^{-3}$ . Turbulent speeds decline from above 100 km/s shortly after the flare to below 50 km/s, as shown in Fig. 10 (Ciaravella and Raymond 2008; Bemporad 2008). The thickness of the current sheet structure at large heights can be far larger than expected from classical theory (Lin et al. 2009; Ciaravella and Raymond 2008; Patsourakos and Vourlidas 2011). That could indicate a turbulent reconnection sheet, and indeed the relation between turbulent speed and current sheet thickness proposed by Lazarian and Vishniac (1999) roughly agrees with the current sheet of the 04 November 2003 flare (Ciaravella and Raymond 2008). On the other hand, the width might reflect the spreading of a Petschek exhaust flow with distance from the diffusion region (Vřsnaek et al. 2009). The Petschek interpretation would also explain why Savage et al. (2010) measured a significantly smaller current sheet width from Hinode XRT X-ray observations at lower heights than Patsourakos and Vourlidas (2011) did at a larger height from coronagraph data for the

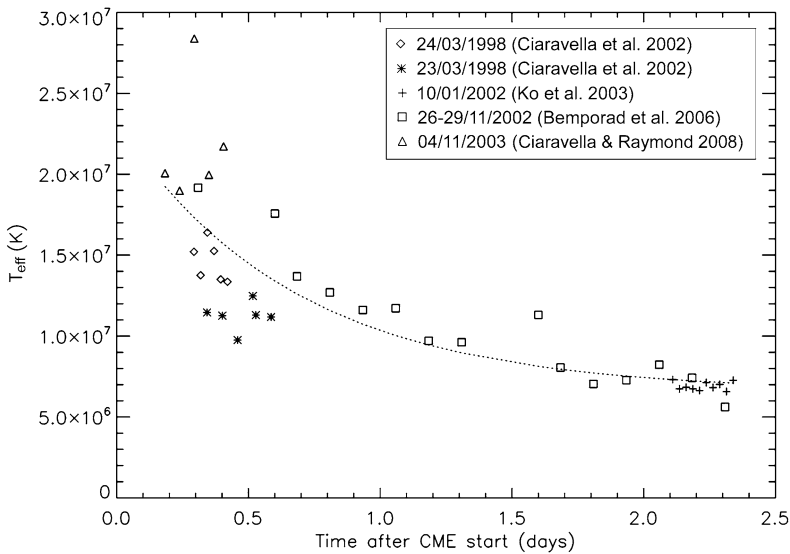


**Fig. 10** Effective temperatures of several current sheets. The effective temperature is given by the line width of the [Fe XVIII] line, which is the quadrature sum of the thermal speed and the turbulent speed (Bemporad 2008)

8 April 2009 event and why Liu et al. (2010) also measure a small current sheet thickness close to the flare loops.

Flow speeds along the current sheet are expected to be near the Alfvén speed, but Savage et al. (2010) measured upflow and downflow speeds of 100 to 170 km/s in a series of Hinode XRT images, apparently emanating from a region whose height increased with time. The observed speeds of supra-arcade downflows (SADs) are much smaller than likely Alfvén speed, suggesting that the features are contracting loops rather than Petschek outflow. The SADs can be either dark or bright (Savage and McKenzie 2011). Plasmoids or “blobs” seen in white light have been used as proxies for the Alfvén speed (Lin et al. 2009), but in the case of the 4 November 2003 event, the blobs are very cool material that moves parallel to the current sheet but not in it (Ciaravella and Raymond 2008).

## 5 Difficulties with the Standard Picture

The standard picture is agnostic about the mechanism of particle acceleration, but it locates the acceleration site in or near the reconnection region in the corona, so that the transport to higher density gas at the chromosphere governs the white light and HXR light curves. Within that context, the observations place strong constraints on mechanisms for particle acceleration and transport.

A significant difficulty for the standard picture is the “number problem.” A large flare produces  $10^{39}$  energetic electrons, which corresponds to the entire electron content of a substantial volume of the corona, perhaps  $10^{30} \text{ cm}^{-3}$  (Simnett 1995). Thus the acceleration mechanism must be extremely efficient if acceleration occurs in the corona, energizing most of the electrons that enter the reconnection region. The total volume of field annihilation and inflowing plasma is far larger than the diffusion region in the Petschek reconnection picture.

In the December 31, 2007 flare, the acceleration region observed in HXR and microwaves above the soft X-ray loops (Krucker et al. 2010) fills a volume of  $\sim 8 \times 10^{26} \text{ cm}^3$ , with  $\sim 2 \times 10^{36}$  electrons above 16 keV. Assuming that these electrons are due to the bulk acceleration of the ambient plasma brought in by magnetic reconnection flows, and that the incoming velocity is  $\sim 0.1 V_A$  (where  $V_A$  is the Alfvén speed), then the rate that electrons are brought into the reconnection region (assumed to arrive from both sides) is  $dN/dt = 2 \times V_A n_e A$ , where  $A$  is the cross sectional area of the inflow. For this flare  $V_A = 2.2 \times 10^8 \text{ cm s}^{-1}$ , and  $dN/dt = 10^{36} \text{ electrons s}^{-1}$ , for a total of  $10^{38}$  electrons in the  $\sim 100 \text{ s}$  duration of the HXR burst. For a very large flare these numbers could well be an order of magnitude larger.

Another problem is that the magnetic reconnection rate for collisional resistivity in the classic “Sweet-Parker” geometry calculated by Parker (1957) (see also Sweet 1969) is many orders of magnitude too slow. The Petschek geometry permits faster reconnection, but requires a localized high resistivity in the diffusion region, or else it relaxes to the slow Sweet-Parker geometry. A new, collisionless (Hall) reconnection process has been identified through theory and simulations, and directly observed in space and in the laboratory [see discussion in Lin et al. (2003) and Cassak et al. (2006) and reviews cited therein]. It should occur under solar coronal conditions with reconnection inflow rates of order  $\sim 0.1 V_A$  (where  $V_A$  is the Alfvén speed). In addition, the particles must be transported to the chromosphere. Given the small footpoint size (HXR footpoints are often unresolved in the direction perpendicular to the flare ribbons, e.g. Krucker et al. 2011b), beam densities must be of order  $10^{10} \text{ cm}^{-3}$ , or about the same as the plasma density, and the enormous current requires a comparable reverse current. The situation is likely to be unstable for large flares (flux  $> 10^{18} \text{ cm}^{-2} \text{ s}^{-1}$ ) and lead to filamentation or to excitation of plasma turbulence, which could impede the transport as in the case of the electric field required to set up the reverse current. The high beam current also requires a large return current, which could excite other instabilities, but the system appears to stabilize quickly and permit beam propagation (Lee and Büchner 2011) (see Zharkova et al. 2011 for a review).

Another potential difficulty with the standard picture is some evidence for isotropic hard X-ray emission based on the predicted effects of reflected photons on the spectrum (Kontar and Brown 2006). In the standard model, photons emitted by the energetic electrons are fairly strongly beamed downwards, leading to a strong reflected component in hard X-rays. Kašparová et al. (2007) studied the dependence of flare X-ray spectra with distance from Sun center in order to infer the albedo contributions. They found that the spectra were consistent with isotropic X-ray emission, but also with strongly beamed emission in the standard picture.

These potential difficulties have led to proposed modifications of the standard picture. Fletcher and Hudson (2008) suggest that reconnection causes rapid contraction of coronal magnetic loops, effectively launching Alfvén waves from the corona along the loops toward the footpoints. These waves can generate strong electric fields as they propagate through steep spatial gradients, potentially accelerating electrons in the chromosphere. Reflection of the Alfvén waves in the chromosphere could also lead to mode conversion and subsequent cascade to high wave numbers, permitting turbulent acceleration of electrons. In either case, the large number of electrons available in the chromosphere avoids the number problem. Another alternative picture is that electrons are accelerated in the corona, but rather than simply depositing their energy in the chromosphere, they are reaccelerated, greatly reducing the number of coronal electrons required (Brown et al. 2009). As an example of a reacceleration mechanism, Brown et al. (2009) develop a picture in which a current sheet cascade produces small scale electric fields that provide stochastic acceleration in the chromosphere. Other ways of re-accelerating electrons include the possibility that after they lose most of

their energy in the chromospheric footpoints, they travel back to the coronal acceleration region where they are reaccelerated (Siversky and Zharkova 2009).

## 6 Summary

Here we summarize the observational characteristics that a model of particle acceleration in solar flares should be able to match. A few of these points assume the ‘standard picture’ of the flare, so that and the other caveats given above should be kept in mind when using these points to assess models.

*Spectrum:* The particles must achieve a power law spectrum or a power law with a break. The spectral index varies with time, often with a *soft-hard-soft* pattern. The behavior at low energies, where thermal emission dominates, is more difficult to determine.

*Energy:* Electrons must reach MeV energies and protons must reach 10 GeV before escaping from the acceleration region simply to reach the observed energies. This is potentially a difficulty for a very thin reconnection region.

*Efficiency:* The acceleration must be very efficient, of order 50 %, in terms of both the fraction of energy dissipated that goes into energetic particles and the fraction of electrons in the reconnection region that undergo acceleration (Emslie et al. 2005; Krucker et al. 2010). The acceleration region must be far larger than the diffusion region in Petschek reconnection.

*Speed:* The acceleration must be very rapid, with a time scale of 0.1 to 1 second in order to match the timescales of X-ray and radio spikes (Dmitriev et al. 2006; Kaufmann et al. 2009). This requires very rapid reconnection in the standard picture.

*Selectivity:* If flares are indeed related to impulsive SEP events, the acceleration mechanism must preferentially accelerate He and especially  $^3\text{He}$ , as well as Fe in order to match *in situ* measurements of impulsive SEPs and remote observations of  $\gamma$ -rays (Vilmer et al. 2011).

*Acceleration region:* In the standard picture, the acceleration occurs in a region with a field of order a hundred Gauss, a density of order  $10^9 \text{ cm}^{-3}$  and a temperature of a few MK. Non-thermal plasma velocities range from  $\sim 100 \text{ km/s}$  well above the main reconnection region to  $\sim 1000 \text{ km/s}$  in the supra-arcade fan (Ciaravella and Raymond 2008; Innes et al. 2003).

Many of the issues discussed above will be addressed in the coming years. Further analysis of existing data will yield better constraints on the models. New observations from the AIA and EVE instruments on SDO are just beginning to be explored and related to physical processes in flares. They provide spectacularly detailed measurements of the location and ionization state of the thermal plasma, which must then be related to plasma heating and energy deposition by accelerated particles. Departures from ionization equilibrium must be taken into account, especially for small events (Bradshaw and Klimchuk 2011).

Both computing power and simulation techniques are advancing rapidly, though it is still difficult to connect the microscopic and macroscopic realms. MHD models can now mimic the main features of flares (Lynch et al. 2008; van der Holst et al. 2009; Riley et al. 2008), and there are several competing models for the particle acceleration process (Lee et al. 2012; Petrosian 2012).

Finally, there are several new instruments on the horizon. The Interface Region Imaging Spectrometer (IRIS) with a launch data of December 2012 will provide high temporal resolution (up to 1 second) and  $0.3''$  spatial resolution of the chromospheric flare ribbons. Although the Frequency-Agile Solar Radiotelescope (FASR) is currently only partially funded,

FASR will image the Sun over a wide radio frequency range as early as 2013. The next X-ray telescope (Spectrometer/Telescope for Imaging X-rays, STIX) will fly on ESA's Solar Orbiter mission (to be launched in 2017). While the sensitivity of STIX will be somewhat greater than that of RHESSI, the main new input into solar flare physics will be achieved by combining the STIX observations from Solar Orbiter's unique viewing angle with X-ray data from an instrument in Earth orbit. A more significant increase in sensitivity and dynamic range of solar hard X-ray imaging observations can be achieved with hard X-ray focusing optics. The Focusing Optics Solar X-ray Imager, FOXSI (Krucker et al. 2011a), a NASA sounding rocket payload to be launched in fall 2012, will provide first results with an enhanced sensitivity of about a factor of 50 compared to RHESSI. Observations with an even higher sensitivity will be provided by the Nuclear Spectroscopic Telescope Array (NuSTAR, Harrison et al. 2010) mission to be launched in 2012. Although designed to observe astrophysical objects, the hard X-ray focusing observatory NuSTAR will provide a few days of solar observations at a 200-fold enhanced sensitivity compared to RHESSI.

In the gamma-ray range, the balloon mission Gamma-Ray Imager/Polarimeter for Solar Flares (GRIPS) will provide the next generation gamma-ray imaging and spectroscopy with an increased sensitivity of about a factor of 5 and angular resolution improvement by a factor of 3 (to  $\sim 12$  arcsec) compared to RHESSI. GRIPS utilizes germanium detectors (3D-GEDs) that locate every energy deposition in 3D to a fraction of a mm, plus a new Multi-Pitch Rotating Modulation (MPRM) for a clean point response function. It also will provide excellent polarization measurements for solar flare X-rays above  $\sim 150$  keV, by tracking the Compton scattering of the incoming photon. GRIPS is planned to be flown on long duration ( $\sim 30$  day) balloon flights from Antarctica in 2014–2016 to catch large solar flares.

Among the new missions being considered for the next solar maximum, the SEE (Solar Eruptive Events) mission is designed to study the huge eruptive events that include both a large flare and a fast CME. These large events are responsible for the acceleration of particles to the highest energies and fluxes, as well as the most intense space weather at the Earth and throughout the heliosphere. SEE will combine a focusing hard X-ray telescope for accelerated, tens of keV electrons with gamma-ray imaging spectroscopy of flare-accelerated ions, plus imaging of newly discovered (Mewaldt et al. 2009) energetic neutral atoms (ENAs) from SEP acceleration high in the corona. Each instrument offers unique insights into the properties of the energetic particle distributions in flares and CMEs. These instruments would be accompanied by context instruments such as a UV coronagraph/spectrometer that would provide the physical conditions (density, temperature, flows, magnetic fields, seed particle distributions, etc.) in the particle acceleration/energy release regions.

**Acknowledgements** J.C.R. was supported by NASA grants NNX09AB17G and NNX11AB61G to the Smithsonian Astrophysical Observatory. S.K. & R.P.L. were supported by NASA contract NAS598033 and NASA grant NNX10AQ31G at UCB; R.P.L. also supported in part by WCU grant (No. R31-10016) funded by the Korean Ministry of Education, Science & Technology.

## References

- M. Ackermann et al., *Astrophys. J.* **745**, 144 (2012)
- S.K. Antiochos, C.R. DeVore, J.A. Klimchuk, *Astrophys. J.* **510**, 485 (1999)
- M.J. Aschwanden, T. Kosugi, H.S. Hudson, M.J. Wills, R.A. Schwartz, *Astrophys. J.* **470**, 1198 (1996)
- H. Aurass, G. Mann, *Astron. Astrophys.* **615**, 526 (2004)
- M. Battaglia, A.O. Benz, *Astron. Astrophys.* **456**, 751 (2006)
- M. Battaglia, A.O. Benz, *Astron. Astrophys.* **487**, 337 (2008)
- A. Bemporad, *Astrophys. J.* **689**, 572 (2008)

- A. Bemporad, G. Poletto, S.T. Suess, Y.-K. Ko, N.A. Schwadron, H.A. Elliot, J.C. Raymond, *Astrophys. J.* **638**, 1110 (2006)
- S.J. Bradshaw, J.A. Klimchuk, *Astrophys. J. Suppl. Ser.* **194**, 26 (2011)
- J.C. Brown, R. Turkmani, E.P. Kontar, A.L. MacKinnon, L. Vlahos, *Astron. Astrophys.* **508**, 993 (2009)
- J.C. Brown, P.C.V. Mallik, N.R. Badnell, *Astron. Astrophys.* **525**, 1 (2010)
- J.W. Brosius, S.M. White, *Astrophys. J. Lett.* **641**, L69 (2006)
- H.V. Cane, R.A. Mewaldt, C.M.S. Cohen, T.T. von Roseninge, *J. Geophys. Res., Atmos.* **111**, A06S90 (2006)
- H. Carmichael, *NASA Spec. Publ.* **50**, 451 (1964)
- A. Caspi, R.P. Lin, *Astrophys. J. Lett.* **725**, L161 (2010)
- P.A. Cassak, J.F. Drake, M.A. Shay, *Astrophys. J. Lett.* **644**, 145 (2006)
- B. Chen, T.S. Bastian (2011). arxiv:[1108.0131](https://arxiv.org/abs/1108.0131) [astro-ph]
- Q. Chen, V. Petrosian (2012). arxiv:[1201.1484](https://arxiv.org/abs/1201.1484) [astro-ph]
- X. Cheng, J. Zhang, Y. Liu, M.D. Ding, *Astrophys. J. Lett.* **732**, L25 (2011)
- A. Ciaravella, J.C. Raymond, *Astrophys. J.* **686**, 1372 (2008)
- A. Ciaravella, J.C. Raymond, J. Li, P. Reiser, L.D. Gardner, Y.-K. Ko, S. Fineschi, *Astrophys. J.* **575**, 1116 (2002)
- A.J. Conway, J.C. Brown, B.A.C. Eves, E. Kontar, *Astron. Astrophys.* **407**, 725 (2003)
- C. Dauphin, N. Vilmer, *Astron. Astrophys.* **468**, 289 (2007)
- B.R. Dennis, A.G. Emslie, H.S. Hudson, *Space Sci. Rev.* **159**, 3 (2011)
- P.B. Dmitriev, I.V. Kudryavtsev, V.P. Lazutkov, G.A. Matveev, M.I. Savchenko, D.V. Skorodumov, Y.E. Charikov, *Sol. Syst. Res.* **40**, 142 (2006)
- J.F. Drake, M. Swisdak, H. Che, M.A. Shay, *Nature* **443**, 553 (2006a)
- J.F. Drake, M. Swisdak, K.M. Schoeffler, B.N. Rogers, S. Kobayashi, *Geophys. Res. Lett.* **33**, L13105 (2006b)
- G.A. Dulk, A.L. Kiplinger, R.M. Winglee, *Astrophys. J.* **389**, 756 (1992)
- A.G. Emslie, B.R. Dennis, G.D. Holman, H.S. Hudson, *J. Geophys. Res., Atmos.* **110**, 11103 (2005)
- A.G. Emslie, B. Dennis, H. Hudson, R. Lin, *High Energy Aspects of Solar Flares: A RHESSI-Inspired Monograph* (2011)
- L.A. Fisk, *Astrophys. J.* **224**, 1048 (1978)
- L. Fletcher, H.S. Hudson, *Astrophys. J.* **675**, 1645 (2008)
- L. Fletcher, I.G. Hannah, H.S. Hudson, T.R. Metcalf, *Astrophys. J.* **656**, 1187 (2007)
- L. Fletcher et al., *Space Sci. Rev.* **159**, 19 (2011)
- P.T. Gallagher, B.R. Dennis, S. Krucker, R.A. Schwartz, K.A. Tolbert, *Sol. Phys.* **210**, 341 (2002)
- S.E. Gibson et al., *Astrophys. J.* **724**, 1133 (2010)
- L. Glesener, S. Krucker, R.P. Lin, *Astrophys. J.* (2012, submitted)
- J.A. Grayson, S. Krucker, R.P. Lin, *Astrophys. J.* **707**, 1588 (2009)
- P.C. Grigis, A.O. Benz, *Astron. Astrophys.* **426**, 1093 (2004)
- J. Guo, S. Liu, L. Fletcher, E. Kontar, *Astrophys. J.* **728**, 4 (2011)
- D.K. Haggerty, E.C. Roelof, *Astrophys. J.* **579**, 841 (2002)
- I.G. Hannah et al., *Space Sci. Rev.* **159**, 263 (2011)
- F.A. Harrison, S. Boggs, F. Christensen et al., *SPIE 7732* (2010)
- E. Haug, *Astron. Astrophys.* **326**, 417 (1997)
- J. Heyvaerts, *Sol. Phys.* **53**, 255 (1975)
- T. Hirayama, *Sol. Phys.* **34**, 323 (1974)
- G.C. Ho, E.C. Roelof, G.M. Mason, *Astrophys. J. Lett.* **621**, 141 (2005)
- R.A. Hock, P.C. Chamberlain, T.N. Woods, D. Crotser, F.G. Eparvier, F.G. Woodraska, E.C. Woods, *Sol. Phys.* **275**, 145 (2010)
- G.D. Holman, M.J. Aschwanden, H. Aurass, M. Battaglia, P.C. Grigis, W. Liu, P. Saint-Hilaire, V.V. Zharkova, *Space Sci. Rev.* **159**, 107 (2011)
- G.D. Holman, L. Sui, R.A. Schwartz, A.G. Emslie, *Astrophys. J. Lett.* **595**, L97 (2003)
- G.D. Holman, M.J. Aschwanden, H. Aurass, M. Battaglia, P.C. Grigis, E.P. Kontar, W. Liu, P. Saint-Hilaire, V.V. Zharkova, *Space Sci. Rev.* **159**, 107 (2011)
- H.S. Hudson, C.J. Wolfson, T.R. Metcalf, *Sol. Phys.* **234**, 79 (2006)
- H.S. Hudson, L. Fletcher, A.L. MacKinnon, T.N. Woods, Preprint (2012)
- G.J. Hurford, S. Krucker, R.P. Lin, R.A. Schwartz, G.H. Share, D.M. Smith, *Astrophys. J. Lett.* **644**, L93 (2006)
- I.A. Ibragimov, G.E. Kocharov, in *Proc. 15th Int. Cosmic Ray Conf.* Plovdiv, vol. 11, p. 340 (1977)
- D.E. Innes, D.E. McKenzie, T. Wang, *Sol. Phys.* **217**, 247 (2003)
- S. Ishikawa, S. Krucker, T. Takahashi, R.P. Lin, *Astrophys. J.* **737**, 48 (2011)
- C.M. Johns, R.P. Lin, *Sol. Phys.* **137**, 121 (1992)

- S.W. Kahler, *Space Sci. Rev.* **129**, 359 (2007)
- J. Kašparová, E.P. Kontar, J.C. Brown, *Astron. Astrophys.* **466**, 705 (2007)
- P. Kaufmann, C.G. Giménez de Castro, E. Correia, E.R. Joaquim, J.-P. Raulin, A.S. Válio, *Astrophys. J.* **697**, 420 (2009)
- M. Kazachenko, R.C. Canfield, D.W. Longcope, J. Qiu, *Sol. Phys.* (2011). doi:[10.1007/s11207-011-9786-6](https://doi.org/10.1007/s11207-011-9786-6)
- A.L. Kiplinger, *Astrophys. J.* **453**, 973 (1995)
- A.L. Kiplinger, R.M. Winglee, *Astrophys. J.* **389**, 756 (1992)
- B. Kliem, T. Török, *Phys. Rev. Lett.* **96**, 255002 (2006)
- Y.-K. Ko, J.C. Raymond, J. Lin, G. Lawrence, J. Li, A. Fludra, *Astrophys. J.* **594**, 1068 (2003)
- E.P. Kontar, J.C. Brown, *Adv. Space Res.* **38**, 945 (2006)
- E.P. Kontar, J.C. Brown, A.G. Emslie, R.A. Schwartz, D.M. Smith, R.C. Alexander, *Astrophys. J. Lett.* **595**, L123 (2003)
- E.P. Kontar, A.G. Emslie, A.M. Massone, M. Piana, J.C. Brown, M. Prato, *Astrophys. J.* **670**, 857 (2007)
- E.P. Kontar, E. Dickson, J. Kašparová, *Sol. Phys.* **252**, 139 (2008)
- E.P. Kontar et al., *Space Sci. Rev.* **159**, 301 (2011)
- R.A. Kopp, G.W. Pneuman, *Sol. Phys.* **50**, 85 (1976)
- S. Krucker, D.E. Larson, R.P. Lin, B.J. Thompson, *Astrophys. J.* **519**, 864 (1999)
- S. Krucker, R.P. Lin, *Sol. Phys.* **210**, 229 (2002)
- S. Krucker, M.D. Fivian, R.P. Lin, *Adv. Space Res.* **35**, 1707 (2005)
- S. Krucker, S.M. White, R.P. Lin, *Astrophys. J.* **699**, L49 (2007)
- S. Krucker, G.J. Hurford, A.L. MacKinnon, A.Y. Shih, R.P. Lin, *Astrophys. J. Lett.* **678**, L63a (2008)
- S. Krucker, P.H. Oakley, R.P. Lin, *Astrophys. J.* **691**, 806 (2009)
- S. Krucker, H.S. Hudson, L. Glesener, S.M. White, S. Masuda, J.-P. Wuelser, R.P. Lin, *Astrophys. J.* **714**, 1108 (2010)
- S. Krucker, S. Christe, L. Glesener et al., *Proc. SPIE* **8147**, 4 (2011a)
- S. Krucker, H.S. Hudson, N.L.S. Jeffrey et al., *Astrophys. J.* **739**, 96 (2011b)
- A. Lazarian, E.T. Vishniac, *Astrophys. J.* **517**, 700 (1999)
- A. Lazarian, G. Kowal, E. de Gouveia Dal Pino, *Planet. Space Sci.* **59**, 537 (2011)
- K.W. Lee, J. Büchner, *Astron. Astrophys.* **353**, 61 (2011)
- M.A. Lee et al., this issue (2012)
- H. Lin, M.J. Penn, S. Tomczyk, *Astrophys. J. Lett.* **541**, L83 (2000)
- J. Lin, T.G. Forbes, *J. Geophys. Res.* **105**, 2375 (2000)
- J. Lin, J.C. Raymond, A.A. van Ballegoijen, *Astrophys. J.* **602**, 422 (2004)
- J. Lin, Y.-K. Ko, J.C. Raymond, *Astrophys. J.* **693**, 1666 (2009)
- R.P. Lin, *Sol. Phys.* **100**, 537 (1985)
- R.P. Lin, *Space Sci. Rev.* **159**, 421 (2011)
- R.P. Lin, H.S. Hudson, *Sol. Phys.* **50**, 153 (1976)
- R.P. Lin et al., *Astrophys. J. Lett.* **595**, L69 (2003)
- Y.E. Litvinenko, *Astron. Astrophys.* **452**, 1069 (2006)
- S. Liu, V. Petrosian, G.M. Mason, *Astrophys. J. Lett.* **613**, L81 (2004)
- S. Liu, V. Petrosian, G.M. Mason, *Astrophys. J.* **636**, 462 (2006)
- W. Liu, V. Petrosian, B.R. Dennis, Y.-W. Jiang, *Astrophys. J.* **676**, 704 (2008)
- R. Liu, J. Lee, T. Wang, G. Stenborg, C. Liu, H. Wang, *Astrophys. J. Lett.* **723**, L28 (2010)
- W. Liu, V. Petrosian, J.T. Mariska, *Astrophys. J.* **702**, 1553 (2009)
- D.W. Longcope, S.E. Guidoni, *Astrophys. J.* **740**, 73 (2011)
- B.J. Lynch, S.K. Antiochos, C.R. DeVore, J.G. Luhmann, T.H. Zurbuchen, *Astrophys. J.* **683**, 1192 (2008)
- G.M. Mason, J.E. Mazur, J.R. Dwyer, *Astrophys. J.* **565**, L51 (2002a)
- G.M. Mason et al., *Astrophys. J.* **574**, 1039 (2002b)
- G.M. Mason, *Space Sci. Rev.* **130**, 231 (2007)
- S. Masuda, T. Sato, T. Kosugi, T. Sakao, *Adv. Space Res.* **26**, 493 (2000)
- S. Masuda, T. Kosugi, H. Hara, S. Tsuneta, Y. Ogawara, *Nature* **371**, 495 (2004)
- D.E. McKenzie, S.L. Savage, *Astrophys. J.* **697**, 1569 (2009)
- R.A. Mewaldt et al., in G. Li, Q. Hu, O. Verkhoglyadova, G.p. Zank, R.P. Lin, J. Luhmann (eds.) *Particle Acceleration in the Heliosphere and Beyond*. AIP Conf. Proc. vol. 1039, Melville, NY (2008), p. 111
- R.A. Mewaldt et al., *Astrophys. J. Lett.* **693**, L11 (2009)
- J.A. Miller, *J. Geophys. Res., Atmos.* **102**, 14631 (1997)
- R.O. Milligan, B.R. Dennis, *Astrophys. J.* **699**, 968 (2009)
- E. Möbius, Y. Cao, M.A. Popecki, L.M. Kistler, H. Kucharek, D. Morris, B. Klecker, in *Proc. 28th Int. Cosmic Ray Conf.* vol. 6, p. 3273 (2003)
- N.A. Murphy, J.C. Raymond, K.E. Korreck, *Astrophys. J.* **735**, 17 (2011)
- R.J. Murphy, C.D. Dermer, R. Ramaty, *Astrophys. J. Suppl. Ser.* **63**, 721 (1987)

- R.J. Murphy, G.H. Share, J.R. Letaw, D.J. Forrest, *Astrophys. J.* **358**, 298 (1990)
- R.J. Murphy, R. Ramaty, B. Kozlovsky, D.V. Reames, *Astrophys. J.* **371**, 793 (1991)
- R.J. Murphy, B. Kozlovsky, G.H. Share, X.-M. Hua, R.E. Lingenfelter, *Astrophys. J. Suppl. Ser.* **168**, 167 (2007)
- F.Q. Orrall, J.B. Zirker, *Astrophys. J.* **208**, 618 (1976)
- B.T. Park, V. Petrosian, R.A. Schwarz, *Astrophys. J.* **489**, 358 (1997)
- E.N. Parker, *J. Geophys. Res.* **62**, 509 (1957)
- S. Patsourakos, A. Vourlidas, *Astron. Astrophys.* **525**, 27 (2011)
- T. Peter, E.N. Ragozin, A.M. Urvov, U.B. Uskov, D.M. Rust, *Astrophys. J.* **351**, 317 (1990)
- V. Petrosian, T.Q. Donaghy, J.M. McTiernan, *Astrophys. J.* **569**, 459 (2002)
- V. Petrosian, Q. Chen, *Astrophys. J. Lett.* **712**, L131 (2010)
- V. Petrosian, T.Q. Donaghy, *Astrophys. J.* **527**, 945 (1999)
- V. Petrosian, S. Liu, *Astrophys. J.* **610**, 550 (2004)
- V. Petrosian, J.M. McTiernan, H. Marschhauser, *Astrophys. J.* **434**, 747 (1994)
- V. Petrosian, Y.W. Jiang, S. Liu, G.C. Ho, G.M. Mason, *Astrophys. J.* **701**, 1 (2009)
- V. Petrosian (2012), this issue, doi:[10.1007/s11214-012-9900-6](https://doi.org/10.1007/s11214-012-9900-6)
- M. Piana, A.M. Massone, G.J. Hurford, M. Prato, A.G. Emslie, E.P. Kontar, R.A. Schwartz, *Astrophys. J.* **665**, 846 (2007)
- M. Pick, N. Vilmer, *Astron. Astrophys. Rev.* **16**, 1 (2008)
- J. Qiu, J. Lee, D.E. Gary, H. Wang, *Astrophys. J.* **565**, 1335 (2002)
- J.C. Raymond, *Astron. Nachr.* (2012, in press)
- J.C. Raymond, G. Holman, A. Ciaravella, A. Panasyuk, Y.-K. Ko, J. Kohl, *Astrophys. J.* **659**, 750 (2007)
- D.V. Reames, *Space Sci. Rev.* **90**, 413 (1999)
- D.V. Reames, L.M. Barbier, T.T. von Roseninge, G.M. Mason, J.E. Mazur, J.R. Dwyer, *Astrophys. J.* **483**, 515 (1997)
- D.V. Reames, J.P. Meyer, T.T. von Roseninge, *Astrophys. J. Suppl. Ser.* **90**, 64 (1994)
- K.K. Reeves, L. Golub, *Astrophys. J. Lett.* **727**, L52 (2011)
- P. Riley, R. Lionello, Z. Mikić, J. Linker, *Astrophys. J.* **672**, 1221 (2008)
- P. Saint-Hilaire, A.O. Benz, *Astron. Astrophys.* **435**, 743 (2005)
- T. Sakao, T. Kosugi, S.I. Masuda, K. Yaji, M. Inada-Koide, K. Makashima, *Adv. Space Res.* **17**, 67 (1996)
- A. Savcheva, E. Parlat, A. van Ballegoijen, G. Aulair, E. DeLuca, *Astrophys. J.* **750**, 15 (2012)
- S.L. Savage, D.E. McKenzie, K.K. Reeves, T.G. Forbes, D.W. Longcope, *Astrophys. J.* **722**, 329 (2010)
- S.L. Savage, D.E. McKenzie, *Astrophys. J.* **730**, 98 (2011)
- C.J. Schrijver, A.M. Title, *J. Geophys. Res., Atmos.* **116**, 04108 (2011)
- C. Shao, G. Huang, *Astrophys. J. Lett.* **694**, L162 (2009)
- G.H. Share et al., *Astrophys. J. Lett.* **595**, L85 (2003)
- K. Shibata, S. Masuda, M. Shimojo, H. Hara, T. Yokoyama, S. Tsuneta, T. Kosugi, Y. Ogawara, *Astrophys. J. Lett.* **451**, L83 (1995)
- A.Y. Shih, R.P. Lin, D.M. Smith, *Astrophys. J. Lett.* **698**, L152 (2009)
- G.M. Simnett, *Space Sci. Rev.* **73**, 387 (1995)
- X. Sun, T. Hoeksema, Y. Liu, T. Weigelmann, K. Hayashi, Q. Chen, J. Thalmann, *Astrophys. J.* **748**, 77 (2012)
- P.A. Sweet, *Annu. Rev. Astron. Astrophys.* **7**, 149 (1969)
- G. Trottet, N. Vilmer, C. Barat, A. Benz, A. Magun, A. Kuznetsov, R. Sunyaev, O. Terekhov, *Astron. Astrophys.* **334**, 1099 (1998)
- T.V. Siversky, V.V. Zharkova, *Astron. Astrophys.* **504**, 1057 (2009)
- K.T. Strong, K. Harvey, T. Hirayama, N. Nitta, T. Shimuzu, S. Tsuneta, *Publ. Astron. Soc. Jpn.* **44**, L161 (1992)
- P.A. Sturrock, *Nature* **211**, 695 (1966)
- L. Sui, G.D. Holman, *Astrophys. J. Lett.* **596**, 251 (2003)
- M. Temmer, A.M. Veronig, E.P. Kontar, S. Krucker, B. Vršnak, *Astrophys. J.* **712**, 1410 (2010)
- T. Török, B. Kliem, *Astrophys. J. Lett.* **630**, 97 (2005)
- D.A. Uzdensky, *Astrophys. J.* **671**, 2139 (2007)
- A.A. van Ballegoijen, P.C.H. Martens, *Astrophys. J.* **343**, 971 (1989)
- B. van der Holst, W. Manchester IV, I.V. Sokolov, G. Tóth, T.O. Gombosi, D. DeZeeuw, O. Cohen, *Astrophys. J.* **693**, 1178 (2009)
- A.M. Veronig, J.C. Brown, *Astrophys. J. Lett.* **603**, L117 (2004)
- N. Vilmer, A.L. MacKinnon, G.J. Hurford, *Space Sci. Rev.* **159**, 167 (2011)
- L. Vlahos, H. Isliker, F. Lepreti, *Astrophys. J.* **608**, 540 (2004)
- A. Vourlidas, R.A. Howard, E. Esfandiari, S. Patsourakos, S. Yashiro, G. Michalek, *Astrophys. J.* **722**, 1522 (2010)



- B. Vršnak, et al., *Astron. Astrophys.* **499**, 905 (2009)
- L. Wang, R.P. Lin, S. Krucker, *Astrophys. J.* **727**, 121 (2011)
- L. Wang, R.P. Lin, S. Krucker, G.M. Mason, *Astrophys. J.* (2012a, submitted)
- L. Wang, R.P. Lin, S. Krucker, G.M. Mason, *Astrophys. J.* (2012b, submitted)
- Y.-M. Wang, M. Pick, G.M. Mason, *Astrophys. J.* **639**, 495 (2006)
- S.M. White et al., *Space Sci. Rev.* **159**, 225 (2011)
- T.N. Woods, F.G. Eparvier, J. Fontenla, J. Harder, G. Kopp, W.E. McClintock, G. Rottman, M. Smiley, M. Snow, *Geophys. Res. Lett.* **31**, L10802 (2004)
- T.N. Woods, G. Kopp, P.C. Chamberlin, *J. Geophys. Res., Atmos.* **111**, 10S14 (2006)
- Y. Xu, A.G. Emslie, G.J. Hurford, *Astrophys. J.* **673**, 576 (2008)
- S. Yashiro, N. Gopalswamy, S. Akiyama, G. Michalek, R.A. Howard, *J. Geophys. Res., Atmos.* **110**, 12S05 (2005)
- T. Yokoyama, K. Akita, T. Morimoto, K. Inoue, J. Newmark, *Astrophys. J. Lett.* **546**, L69 (2001)
- J. Zhang, K.P. Dere, R.A. Howard, A. Vourlidas, *Astrophys. J.* **604**, 420 (2004)
- V.V. Zharkova et al., *Space Sci. Rev.* **159**, 357 (2011)